Surface uplift and time-dependent seismic hazard due to fluid-injection in eastern Texas

One-sentence summary: Observations of surface deformation constrain the extent of pore pressure changes and seismic hazard potential caused by wastewater injection.

Manoochehr Shirzaei

School of Earth and Space Exploration, Arizona State University, Tempe, AZ, USA

Correspondence: shirzaei@asu.edu

William Ellsworth

Department of Geophysics, Stanford University, Stanford, CA USA

Kristy Tiampo

Department of Earth Sciences, University of Western Ontario, London, ON Canada

Canada; now at Cooperative Institute for Research in Environmental Sciences (CIRES) and Department of Geological Sciences, UCB 216, University of Colorado, Boulder, USA

Pablo J. González

COMET and Institute of Geophysics and Tectonics. School of Earth and Environment. University of Leeds. LS2 9JT, Leeds, UK. Now at: COMET and Department of Earth, Ocean and Ecological Sciences, University of Liverpool, Liverpool L69 3GP, UK

Michael Manga

Department of Earth and Planetary Science, University of California, Berkeley, Berkeley, CA USA

Increasing seismicity in the central USA since 2009 coincides in space and time with wastewater injection. However, observations of the surface deformation and physical models to constrain the extent to which fluid migrates and to unequivocally link the seismicity and wastewater injection are scarce. Here we show that wastewater injection in eastern Texas causes uplift at a few mm/year, detectable using radar interferometric data. Using the measured uplift, reported injection data, and a poroelastic model, we compute the complex evolution of crustal strain and pore pressure. We infer that > 1 MPa increase in pore pressure in rocks with low compressibility triggers earthquakes including the M_w4.8, 17 May 2012 event, the largest earthquake recorded in east Texas. Observations that only deeper wells are associated with earthquakes, whereas large pressure change in more shallow aquifers are not, highlights the importance of hydrogeology. The frequency and magnitude of earthquakes increased, even while the injection rates declined, owing to diffusion of pore pressure from earlier periods with higher injection rates. This study shows that surface deformation data are useful to evaluate the evolution of pore pressure and earthquake potential in the vicinity of injection sites.

Introduction

In recent years the eastern and central USA have experienced a sharp increase in the number of earthquakes, with more than 1570 M ≥3 events between 2009 and 2015 (*1-3*). Many of these events occurred near injection disposal wells and the seismicity was preceded by a high rate of fluid injection over a period of months to years, suggesting a link between seismicity and injection operations (*1, 3-8*). In general, earthquake hazard is proportional to the seismic rate, thus the current increase in the seismic rate implies an elevated hazard in the central and eastern US (*9*).

On 17 May 2012, the city of Timpson, Texas, experienced a M_w4.8 earthquake, the largest recorded event in the region (Fig. 1a). This event was preceded and followed by several earthquakes located on a NW-SE trending basement fault including three with $M_w \geq 4.0$ over the following 16 months. Focal depths were shallow, ranging from 1.6 to 5.0 km, with the majority of the strain release between 3.5 and 5 km (*5*). Four Class II disposal wells are located in the vicinity of these earthquakes (Table S1). They dispose co-produced saline formation water from oil and gas production operations in the area by injecting into Lower Cretaceous limestones within the Sabine Uplift of East Texas (*10*). There is no significant production in the immediate area of the disposal wells or the earthquakes. These wells began injection between 2005 and 2007 at a net average rate of $8.9 \times 10^{+5}$ m^3/yr until mid-2012, when injection drops to $7.2 \times 10^{+5}$ m^3/yr in the following years (*5*).

The proximity of the earthquake clusters to the injection wells suggests a link between them (*5, 11*). As wastewater is injected into the disposal formation, it increases pore pressure within the connected hydrologic system. Over time, the pressure perturbation can spread to distances of many km (*12, 13*). The increase in pore pressure due to the injection of fluids decreases the effective normal stress on faults, bringing them closer to failure (*14, 15*) as well as locally inducing stress within the reservoir and surrounding rocks (*16-18*). Moreover, pore pressure increase can cause surface deformation (*18*), measurable using geodetic tools (*19*) and providing the possibility of documenting subsurface evolution from the surface.

Results

To obtain a detailed image of the surface uplift caused by injection, we apply a multitemporal interferometric synthetic aperture radar (InSAR) approach (*20*) to three overlapping sets of L-band SAR images (Tables S2 & S3) acquired by ALOS satellite over the Timpson area during 2007/05/06

and 2010/11/14 (Fig. 1a). High quality interferograms were generated from this L-band data (Fig. S1). Estimating the linear velocity using a large number of interferograms improves the signal-to-noise-ratio of the measurements (see supplementary materials). Velocity maps obtained for each individual data set, as well as the combined map, are consistent and reveal up to 3 mm/yr of uplift in line-of-sight (LOS) over the area between the injection wells (Fig. 1b). Assuming an elastic material with a Poisson's ratio of 0.23 - 0.33 estimated from seismic velocities profiles (see supplementary materials), we estimate that the rate of volume increase under the LOS velocity surface is $8 \times 10^{+5} - 10 \times 10^{+5}$ m^3/yr, consistent with the net injected volume rate at the injection wells. To further validate these results and evaluate the current state of ground deformation, we also applied the same processing scheme to eight C-Band images acquired by the RadarSAT-2 satellite during 2014/03/06 and 2014/08/21 (Fig. S2, Tables S4 & S5). While the location of a zone of maximum deformation is consistent with that obtained from the L-Band data, its spatial extent is broader and the maximum uplift is about 5 mm over ~6 month interval.

The two western wells, W1 and W2, inject at a depth of 1800 m into Trinity Group formations, a porous and permeable limestone that is overlain by the regionally-extensive and impermeable Ferry Lake Anhydrite. The east wells, E1 and E2, inject into carbonate formations of the Washita Group at a depth of 900 m, stratigraphically above the Ferry Lake Anhydrite. The monthly time series of injected volume at each of the injection sites is shown in Figure 1c.

The pressure change due to injection is the likely cause of the surface uplift. To characterize the associated volume strain, we apply an inverse modeling scheme (*21*). To this end, the volume beneath the half space is discretized into rectangular prisms, 3x3 km in area by 0.2 km high between the surface and a depth of 5 km. Within each prism the volume strain is assumed constant (see supplementary materials). Figure S3 shows the observed and modeled deformation rates as well as the associated misfits, indicating that the optimum strain model accurately reproduces the observed

deformation data, with an RMSE of 0.1 mm/yr. The estimated total volume change rate is $7 \times 10^{+5} \pm 1.6 \times 10^{+3}$ m^3/yr, slightly lower than the injection rate. This discrepancy is likely due to diffusion of injected fluids into the surrounding rocks without generating any measureable deformation. We also find a maximum volume strain rate of ~1.5×10^{-6} yr^{-1}, at a depth of 0.8 - 1.1 km adjacent to wells E1 and E2 (Fig. 2a).

The availability of geological profiles and distribution of hydraulic conductivity and Poisson's ratios, allow us to characterize parameters of a poroelastic layered Earth model (Table S5). Using this Earth model and the time series of injected fluid volume, we solve for the evolution of the pore pressure in the crust (see supplementary materials). Figure (2b) shows the 3D distribution of the pore pressure accumulated between 2006 and 2012. We identify two zones of maximum pore pressure at depths of ~0.85 km and ~1.85 km depth near east and west wells, respectively. The shallower zone of elevated pore pressure also coincides with the zone of maximum volume strain. Higher pressures occur between the two west wells where uplift was negligible.

To investigate the relationship between pore pressure distribution associated with injection and the observed seismicity, we estimate the pore pressure increase at the location of the 2012 seismic events, where the main events nucleated between 3.5 and 4.5 km depth (*5*). Overall, fluid injection causes a pore pressure increase of 0.5-1.5 MPa at the hypocentral depth. Pressure changes of this magnitude trigger earthquakes elsewhere (*22*). In the context of Mohr circle stress analysis, a localized increase in pore pressure shifts the circle to the left (i.e., reduces the effective normal stress) and changes its radius (i.e., increases the shear stress), while a homogeneous pore pressure increase only shifts the circle to the left until it touches the failure envelope (*23*). Given the lack of historical large earthquakes in the region and the five year delay between the initiation of injection and the first large event, we suggest that a decrease in effective normal stress (due to a homogeneous increase in pore pressure) together with an increase in shear stress triggered seismicity. The second

119 condition is only satisfied when the pore pressure increase is localized. It is also possible that the
120 initiating seismicity and associated stress change transiently enhanced the permeability (*24-27*),
121 increasing the pore pressure at the location of the deeper events, which in turn promoted further
122 earthquakes.
123
124 **Discussion**
125 We investigated injection from two pairs of wells that began injecting at approximately the
126 same time, disposing approximately the same volumes of wastewater. The main differences are
127 depth of injection and the presence of an impermeable barrier below the shallower east wells that
128 blocks fluid and pressure from reaching deeper formations. The deeper west wells are associated
129 with the 2012 Timpson earthquake sequence, while no detected seismicity occurred near the east
130 wells. This observation highlights the importance of hydrogeology (and geology) for the
131 consequences of fluid injection.
132 The extent to which induced pore pressure change occurs is an important parameter
133 required for accurate estimate of seismic hazards. From regulatory perspective, however,
134 constraining this parameter is not trivial due to its complex relationship with local hydrology (*28*).
135 Using deformation data we are able to put a lower bound on the extent of the rock volume change
136 caused by pore pressure increase. Measurable uplift more than 8 km from the east wells
137 demonstrates the long reach of pressure perturbations inferred in other studies (12, 13, 15).
138 Studies of potentially induced earthquakes suggest that the majority of seismicity occurs
139 within basement rocks, even though most of the injection is done in more shallow sedimentary
140 layers (*2-5, 7, 29, 30*). Of note here is that while pore pressure increased significantly adjacent to
141 both of the east and west wells, little surface deformation was detected in the vicinity of the west
142 wells, where the seismicity occurred (Fig. 2). This is likely due to lower rock compressibility near

143 west wells compared to that of east wells, a feature not accounted for in modeling the evolution of
144 pore pressure, in addition to the greater injection depth. Moreover, injection in the east wells is done
145 in a shallow layer, typically characterized by velocity strengthening frictional properties, thus pore
146 pressure changes are less likely to initiate seismic rupture. We also note the asymmetric pattern in
147 the uplift signal, which cannot be explained by standard models of radial diffusion in a homogenous
148 medium.

149 Figure 3a shows the time series of the maximum pore pressure change at various depths.
150 We note a delayed downward propagation of the pore pressure and that the period of elevated
151 seismicity between 2010 and 2014 coincides with the period of maximum pore pressure change of 1-
152 2.5 MPa at the average depth of 3 km. Though all events coincide with the period of pore pressure
153 increase in the focal zone, the onset of the main sequence in May 2012 corresponds to pressures of
154 about 1 MPa reaching the focal zone (Fig. 3b).

155 The frequency and magnitude of events reached a climax between May 2012 and September
156 2013, when more than 80% of events occurred, including four M_w4+ earthquakes. This period of
157 elevated seismic activity follows a rapid decline in injection at the west wells (Fig. 3b). Thus, the
158 timing of seismicity may result from pore pressure diffusion to the depths of the earthquakes. There
159 are additional contributions to the stresses that may promote seismicity from the poroelastic stresses
160 near the well that accompany the decrease in injection. For an optimally oriented strike-slip fault
161 with fault-normal radial to the injection site, a sudden decline in injection rate relaxes the
162 compressive stress (*31*). All of the seismic events here occurred on a fault with fault-normal oriented
163 at N60^{o}E radial to the west injection wells.

164 Our coupled flow and poroelastic model allows us to predict the future pore pressure
165 distribution after injection ends (Figure 3a). We notice that as injection ends in west wells by about
166 2016, the pressure decreases approximately exponentially. However, the decay rate is fastest in the

most permeable formations and at the depths where injection occurs. At the east wells, 10 years after shut off, the pore pressure remains close its maximum level. For the west wells, only 5 years after the shut off pore pressure drops to the less than 10% of its maximum value. This observation has direct implication for future injection operations and seismic hazard. Changes in the seismicity rate is a function of changes in Coulomb stress and background stress (*32*) and as it is shown here the background stress is characterized by a relaxation time that depends on both the injection history and hydrogeological properties. Thus injection history at a given site may modify future estimates of the seismic hazard.

A better understanding of the earthquake potential from injection-induced seismicity is critically important to assessing the associated hazard. Better quantification of the evolution of the stress and pore pressure in the crust is vital to forecast fault activation (*9*). In addition, a better quantification of the evolution of the stress and pore pressure in the crust may help forecast fault reactivation (*33*). Despite improvements to seismic monitoring capacity and the resulting decrease in the magnitude detection threshold (*34, 35*), observations of the in-situ pore pressure and stress field remain elusive due to scarcity of deformation observations and integration of observations with physical models. This work highlights the value of monitoring surface deformation, in particular using advanced remote sensing techniques, to understand the evolution of pore pressure and stress at depth. The ability to measure crustal stress evolution presents a proactive approach to managing hazard associated with fluid injection. Observation of the time-dependent stress field permits the construction of temporally variable statistical frameworks (*31*), which are useful for earthquake operational forecasting (*36*). The key to successful operational earthquake forecasting is being able to continuously update information about the probability of a future earthquake, which can be achieved using data and models such as those presented in this study. Geodetic monitoring and modeling schemes are valuable components for induced seismic hazard mitigation efforts.

Acknowledgments

RADARSAT-2 images were acquired under SOAR-E project 5226 from the Canadian Space Agency. ALOS data are obtained through Alaska SAR Facilities. Shirzaei's contribution is supported by National Science Foundation grants EAR-1357079 and United States Geological Survey grant G13AP00040. K. Tiampo was supported by an NSERC Discovery Grant. Ellsworth was supported by the Stanford Center for Induced and Triggered Seismicity. Manga is supported by National Science Foundation grants EAR-1344424.

References

1. J. L. Rubinstein, A. B. Mahani, Myths and Facts on Wastewater Injection, Hydraulic Fracturing, Enhanced Oil Recovery, and Induced Seismicity. *Seismological Research Letters* **86**, 1060 (Jul-Aug, 2015).
2. M. Weingarten, S. Ge, J. W. Godt, B. A. Bekins, J. L. Rubinstein, High-rate injection is associated with the increase in US mid-continent seismicity. *Science* **348**, 1336 (Jun 19, 2015).
3. M. J. Hornbach *et al.*, Causal factors for seismicity near Azle, Texas. *Nature communications* **6**, (2015).
4. K. M. Keranen, H. M. Savage, G. A. Abers, E. S. Cochran, Potentially induced earthquakes in Oklahoma, USA: Links between wastewater injection and the 2011 Mw 5.7 earthquake sequence. *Geology* **41**, 699 (2013).
5. C. Frohlich *et al.*, The 17 May 2012 M4.8 earthquake near Timpson, East Texas: An event possibly triggered by fluid injection. *Journal of Geophysical Research: Solid Earth* **119**, 581 (2014).
6. C. Frohlich, E. Potter, C. Hayward, B. Stump, Dallas-Fort Worth earthquakes coincident with activity associated with natural gas production. *The Leading Edge*, 0 (2010).
7. S. Horton, Disposal of Hydrofracking Waste Fluid by Injection into Subsurface Aquifers Triggers Earthquake Swarm in Central Arkansas with Potential for Damaging Earthquake. *Seismological Research Letters* **83**, 250 (2012).
8. F. R. Walsh, M. D. Zoback, Oklahoma's recent earthquakes and saltwater disposal. *Science advances* **1**, e1500195 (2015).
9. W. L. Ellsworth, Injection-Induced Earthquakes. *Science* **341**, (2013).
10. W. H. Granata, "CRETACEOUS STRATIGRAPHY AND STRUCTURAL DEVELOPMENT OF THE SABINE UPLIFT AREA, TEXAS AND LOUISIANA" (Shreveport Geological Society, 1963).
11. Z. Fan, P. Eichhubl, J. F. Gale, Geomechanical analysis of fluid injection and seismic fault slip for the M4. 8 Timpson, Texas, earthquake sequence. *Journal of Geophysical Research: Solid Earth* **in press**, (2016).
12. P. A. Hsieh, J. D. Bredehoeft, A RESERVOIR ANALYSIS OF THE DENVER EARTHQUAKES - A CASE OF INDUCED SEISMICITY. *Journal of Geophysical Research* **86**, 903 (1981, 1981).
13. K. M. Keranen, M. Weingarten, G. A. Abers, B. A. Bekins, S. Ge, Sharp increase in central Oklahoma seismicity since 2008 induced by massive wastewater injection. *Science* **345**, 448 (Jul 25, 2014).
14. C. B. Raleigh, J. H. Healy, J. D. Bredehoeft, An Experiment in Earthquake Control at Rangely, Colorado. **191**, 1230 (1976).
15. Y. Zhang *et al.*, Hydrogeologic Controls on Induced Seismicity inCrystalline Basement Rocks Due to Fluid Injection into Basal Reservoirs. *Ground Water* **51**, 525 (Jul, 2013).
16. P. Segall, Stress and Subsidence Resulting from Subsurface Fluid Withdrawal in the Epicentral Region of the 1983 Coalinga Earthquake. *Journal of Geophysical Research-Solid Earth and Planets* **90**, 6801 (1985).
17. J. Du, J. E. Olson, A poroelastic reservoir model for predicting subsidence and mapping subsurface pressure fronts. *Journal of Petroleum Science and Engineering* **30**, 181 (Sep, 2001).
18. Z. R. Chen, Poroelastic model for induced stresses and deformations in hydrocarbon and geothermal reservoirs. *Journal of Petroleum Science and Engineering* **80**, 41 (2011).
19. D. W. Vasco *et al.*, Satellite-based measurements of surface deformation reveal fluid flow associated with the geological storage of carbon dioxide. *Geophysical Research Letters* **37**, (Feb, 2010).
20. M. Shirzaei, A Wavelet-Based Multitemporal DInSAR Algorithm for Monitoring Ground Surface Motion. *Ieee Geoscience and Remote Sensing Letters* **10**, 456 (May, 2013).
21. A. Mossop, P. Segall, Volume strain within The Geysers geothermal field. *Journal of Geophysical Research-Solid Earth* **104**, 29113 (Dec 10, 1999).
22. E. A. Roeloffs, in *Advances in Geophysics,* R. Dmowska, Ed. (Academic Press, San Diego, 1996).
23. A. Y. Rozhko, Y. Y. Podladchikov, F. Renard, Failure patterns caused by localized rise in pore-fluid overpressure and effective strength of rocks. *Geophysical Research Letters* **34**, (2007).

24. S. Rojstaczer, S. Wolf, PERMEABILITY CHANGES ASSOCIATED WITH LARGE EARTHQUAKES - AN EXAMPLE FROM LOMA-PRIETA, CALIFORNIA. *Geology* **20**, 211 (Mar, 1992).
25. Y. Kitagawa, K. Fujimori, N. Koizumi, Temporal change in permeability of the rock estimated from repeated water injection experiments near the Nojima fault in Awaji Island, Japan. *Geophysical Research Letters* **29**, (May 15, 2002).
26. E. A. Roeloffs, Hydrologie precursors to earthquakes: A review. *Pageoph* **126**, 177 (1988).
27. E. E. Brodsky, E. Roeloffs, D. Woodcock, I. Gall, M. Manga, A mechanism for sustained groundwater pressure changes induced by distant earthquakes. *J. Geophys. Res.* **108**, (2003).
28. S. A. Shapiro, P. Audigane, J.-J. Royer, Large-scale in situ permeability tensor of rocks from induced microseismicity. *Geophys. J. Int.* **137**, 207 (1999).
29. L. Seeber, J. G. Armbruster, W.-Y. Kim, A fluid-injection-triggered earthquake sequence in Ashtabula, Ohio: implications for seismogenesis in stable continental regions. *Bulletin of the Seismological Society of America* **94**, 76 (2004).
30. C. Nicholson, E. Roeloffs, R. L. Wesson, The northeastern Ohio earthquake of 31 January 1986: Was it induced? *Bull. Seism. Soc. Am.* **78**, 188 (1988).
31. P. Segall, S. Lu, Injection-induced seismicity: Poroelastic and earthquake nucleation effects. *Journal of Geophysical Research-Solid Earth* **120**, 5082 (Jul, 2015).
32. J. H. Dieterich, A constitutive law for rate of earthquake production and its application to earthquake clustering. *J. Geophys. Res.* **99**, 2601 (1994).
33. M. W. McClure, R. N. Horne, Pressure Transient Analysis of Fracture Zone Permeability at Soultz-sous-Forêts. *GRC Transactions* **35**, (2011).
34. N. Deichmann, D. Giardini, Earthquakes Induced by the Stimulation of an Enhanced Geothermal System below Basel (Switzerland). *Seismological Research Letters* **80**, 784 (2009).
35. W.-Y. Kim, Induced seismicity associated with fluid injection into a deep well in Youngstown, Ohio. *Journal of Geophysical Research: Solid Earth* **118**, 3506 (2013).
36. T. H. Jordan *et al.*, Operational Earthquake Forecasting: State of Knowledge and Guidelines for Utilization. *Annals of Geophysics* **54**, 315 (2011, 2011).

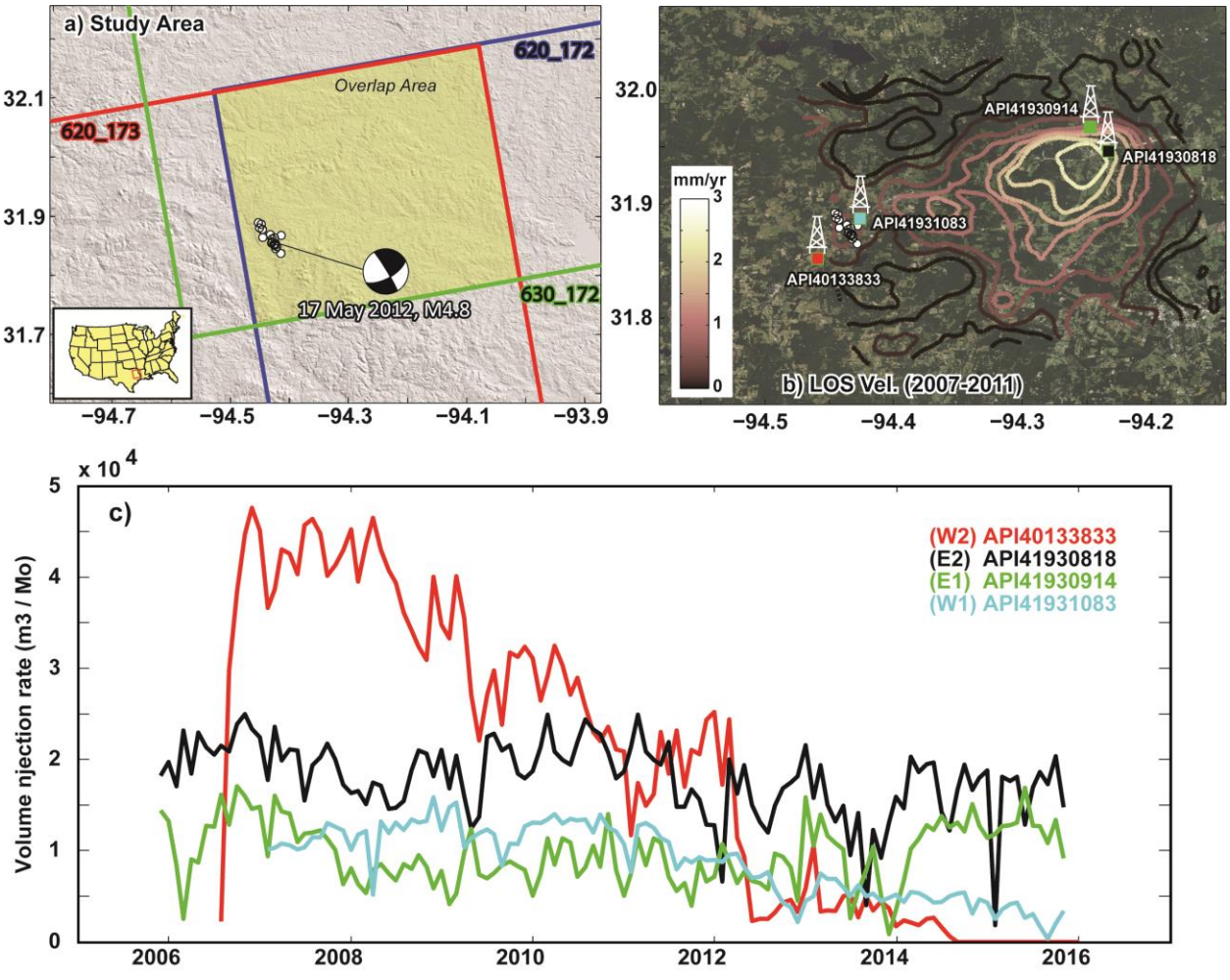

Figure 1. Study area and data sets. a) Three overlapping frames of ALOS satellite in ascending orbit (heading = 350°, incidence = 34.5°). Locations of seismicity and focal mechanism of the Timpson sequence are shown (white dots). b) LOS deformation velocity field obtained from multitemporal processing of the overlapped ALOS SAR data set. Background is the satellite image of the study area, courtesy Google Earth. c) Time series of the volume of injected fluid for each of the wells shown in panel (b). (Mo = month)

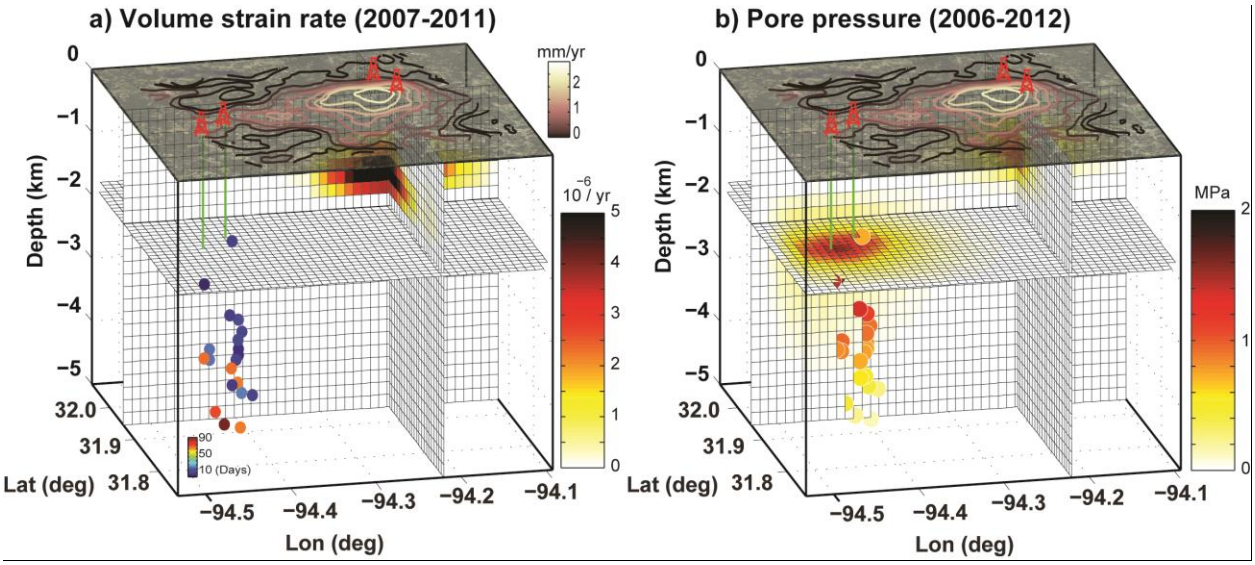

Figure 2. Volumetric strain and pore pressure change. a) Distribution of the estimated volume strain rate. Colored circles show the time of earthquakes with respect to the first event. The injection wells are also shown by green bars. Contour lines show the surface deformation rate b) Distribution of the cumulative pore pressure change between 2006 and 2013. Colored circles show the pore pressure increase at the location of earthquakes.

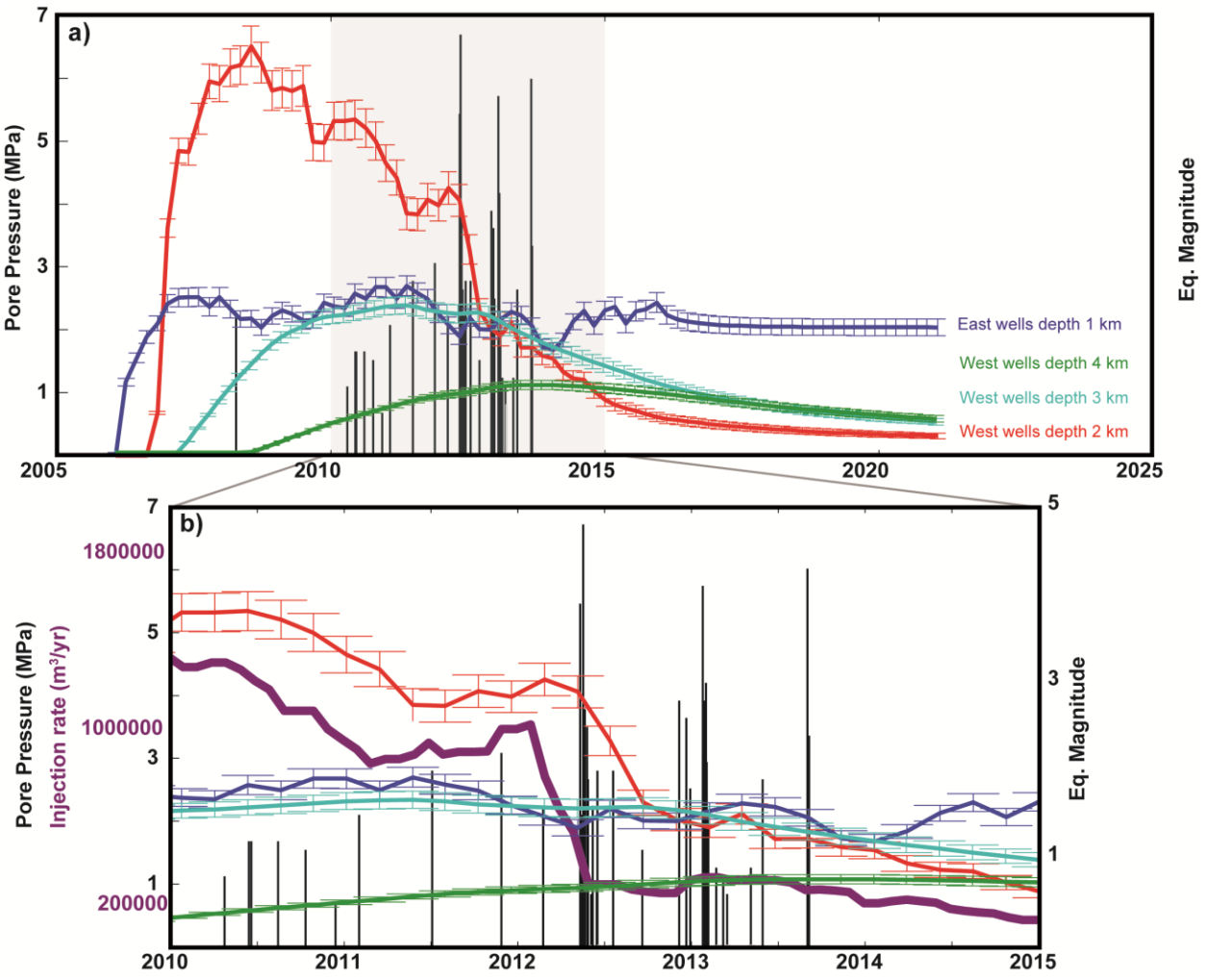

Figure 3. Pore pressure time series. a) Colored lines show time series of pore pressure change at various depths. The errorbars are 1-σ uncertainty and obtained through bootstrapping. Vertical black lines show the time and magnitude of earthquakes in the Timpson sequence (Table S7). b) Zoom of the period 2010-2015 from panel a. The injection rate of the west wells is superimposed in purple.